Cycling With Functional Electrical Stimulation and Adaptive Neural Network Admittance Control

Christian A. Cousin*, Patryk Deptula*, Courtney A. Rouse*, and Warren E. Dixon*

Abstract—For individuals with neurological conditions (NCs) affecting the muscles of their legs, motorized functional electrical stimulation (FES) cycling is a rehabilitation strategy which offers numerous health benefits. Motorized FES cycling is an example of cooperative physical human-robot interaction where both the cycle's motor and rider's muscles (through electrical stimulation) must be well controlled to achieve desired performance. Since every NC is unique, adaptive control of motorized FES cycling is motivated over a one-size-fits-all approach. In this paper, a robust sliding-mode controller is employed on the rider's muscles while an adaptive neural network admittance controller is employed on the cycle's motor to preserve rider comfort and safety. Through a Lyapunov-like switched systems stability analysis, global asymptotic stability of the cycle controller is guaranteed and the muscle controller is proven to be passive with respect to the cycle. Experiments on one able-bodied participant were conducted to validate the control design.

Index Terms—Functional electrical stimulation (FES), Rehabilitation robot, Lyapunov, Admittance, Passivity

I. INTRODUCTION

Within the United States (US), there are an estimated 2.5 million new cases of traumatic brain injury (TBI) [1], 800,000 cases of stroke [2], and nearly 18,000 cases of spinal cord injury (SCI) [3] every year. Additionally, it is reported that there are 3.17 million people within the US with permanent disability from TBI [1] and 285,000 people with a spinal cord injury [3]. Neurological conditions (NCs) such as these, as well as diseases (e.g., Parkinson's, etc.) and other congenital disorders (e.g., cerebral palsy, spina bifida, etc.) can severely impact a person's neuromuscular system, causing paresis/paralysis [1]-[3], and significantly affect their activities of daily living. Consequently, these individuals are at an increased risk of negative secondary health effects such as obesity, heart disease, and diabetes unless they participate in some form of rehabilitative therapy such as motorized functional electrical stimulation (FES) cycling which has been shown to positively impact motor control, muscle strength, and bone mineral density (cf. [4], [5]), etc.

Motorized FES cycling utilizes neuromuscular electrical stimulation to apply electricity to targeted muscle groups on

the legs to induce artificial, involuntary muscle contractions to pedal a cycle in conjunction with an electric motor [6]. Although FES cycling is a safe (e.g., no risk of falling) and convenient rehabilitation option for many people, when applied in practice, it is commonly applied open-loop. However, it is well known that muscle dynamics exhibit highly nonlinear, time-varying, and uncertain dynamics [6] while FES results in nonphysiological muscle recruitment, and poor coordination of the muscle groups [7]. Hence, closedloop control is required to produce accurate regulation of generated movements [8]. Furthermore, because each NC is unique, not only is the need to utilize closed-loop control motivated, but the use of adaptive control as well. While past results such as [6], [9], [10] have utilized robust closedloop methods, others have utilized learning-based methods such as neural networks (NN), fuzzy logic, and repetitive learning controllers to improve cadence/torque tracking of FES cycling, but few conduct or include a rigorous stability analysis (cf. exceptions in [6], [9]-[13]).

A stability analysis is required because it is well known that people with NCs possess a weakened/impaired musculoskeletal system and the utmost care must be taken to avoid further injury when participating in robotic rehabilitation [14], such as FES cycling. In other rehabilitation settings (cf. [15], [16]), safety has been introduced through admittance control [17], which artificially injects interaction dynamics between the human and robot. While admittance control is traditionally viewed as a safer alternative than robust control in terms of physical human-robot interaction [18], a stability analysis remains necessary to demonstrate safe interaction between the human and robot. Thus, passivity is utilized to demonstrate the robot is energetically dissipative with respect to the human and will behave stably [19].

In this paper, physical human-robot interaction for motorized FES cycling is accomplished through the use of multiple controllers employed on the cycle's motor and rider's leg muscles (i.e., quadriceps, hamstrings, and gluteals). The rider's muscles are stimulated through a robust sliding-mode controller, which is guaranteed to be passive with respect to the cycle to ensure rider safety. In comparison to past works by the authors (cf. [20]–[22]), instead of robustly rejecting the torque impressed by the human while maintaining stability and passivity, this result activates the cycle's motor using an asymptotically stable adaptive NN admittance controller, constructed by combining a gradient adaptive term to compensate for the linear-in-the-parameter (LP) dynamics and a NN feedforward term to account for

^{*}Department of Mechanical and Aerospace Engineering, University of Florida, Gainesville FL 32611-6250, USA Email: {ccousin, pdeptula, courtneyarouse, wdixon}@ufl.edu

This research is supported in part by NSF award numbers DGE-1842473 and 1762829. Any opinions, findings and conclusions, or recommendations expressed in this material are those of the author(s) and do not necessarily reflect the views of the sponsoring agency.

the unknown muscle control effectiveness of the rider's muscles. Merging a passive muscle stimulation controller with an asymptotically stable adapting NN admittance controller allows for accurate control of the motorized FES cycle while preserving rider comfort and safety. The designed controller is validated through experiments conducted on one able-bodied participant and indicate the proposed controller offers improved performance with the feedforward adaptive compensation terms when compared to the same feedback-only controller.

II. DYNAMICS

A. Cycle-Rider System

The nonlinear, uncertain cycle-rider dynamics are modeled as ¹

$$M(q)\ddot{q} + C(q,\dot{q})\dot{q} + G(q) + P(q,\dot{q}) + b\dot{q} + d(t) = \underbrace{\sum_{m \in \mathcal{M}} b_m(q,\dot{q})\sigma_m(q)u_h(t) + \underbrace{B_e u_e(t)}_{\tau_e(t)}}_{t_e(t)}, \quad (1)$$

where $q: \mathbb{R}_{\geq 0} \to \mathcal{Q}$ denotes the measurable crank angle, the set $\mathcal{Q} \subseteq \mathbb{R}$ contains all possible crank angles, $\dot{q}: \mathbb{R}_{>0} \to \mathbb{R}$ denotes the calculable velocity, and $\ddot{q}: \mathbb{R}_{>0} \to \mathbb{R}$ denotes the non-measurable acceleration [6]. The torque from the rider's muscles is denoted by $\tau_m: \mathcal{Q} \times \mathbb{R} \times \mathbb{R}_{\geq 0} \to \mathbb{R}$, and the torque from the cycle's electric motor by $\tau_e: \mathbb{R}_{\geq 0} \to \mathbb{R}$. The inertial, centripetal-Coriolis, and gravitational effects of the combined cycle-rider system are denoted by $M: \mathcal{Q} \to \mathbb{R}$, $C: \mathcal{Q} \times \mathbb{R} \to \mathbb{R}$, and $G: \mathcal{Q} \to \mathbb{R}$, respectively. The rider's passive viscoelastic tissue torques and the cycle's friction are denoted by $P: \mathcal{Q} \times \mathbb{R} \to \mathbb{R}$ and $b \in \mathbb{R}_{>0}$, respectively. System disturbances are denoted by $d: \mathbb{R}_{\geq 0} \to \mathbb{R}$. The individual muscle control effectiveness is denoted by $b_m: \mathcal{Q} \times \mathbb{R} \to \mathbb{R}_{>0}$, and the piecewise right-continuous switching signals for activating the individual muscle groups are denoted by $\sigma_m: \mathcal{Q} \to \{0, 1\}, \forall m \in \mathcal{M}$, where the set $\mathcal{M} \triangleq \left\{ RQ \ LQ \ RH \ LH \ RG \ LG \right\}$ includes the right (R) and left (L) quadriceps femoris (Q), hamstring (H), and gluteal (G) muscle groups (i.e., the stimulated muscle groups). The subsequently designed muscle control input is utilized across all muscle groups and is denoted by $u_h: \mathbb{R}_{\geq 0} \to \mathbb{R}$. The known motor control constant relating the motor's input current to output torque is denoted by $B_e \in \mathbb{R}_{>0}$, and the subsequently designed motor control current is denoted by $u_e:\mathbb{R}_{\geq 0}\to\mathbb{R}$. To facilitate further analysis, a lumped switched muscle control effectiveness is denoted by $B_m: \mathcal{Q} \times \mathbb{R} \to \mathbb{R}_{>0}$ and defined as

$$B_{m} \triangleq \sum_{m \in \mathcal{M}} b_{m} (q, \dot{q}) \sigma_{m} (q).$$
 (2)

¹For notational brevity, all explicit dependence on time, t, within the states q(t), $\dot{q}(t)$, $\ddot{q}(t)$ is suppressed.

The right-continuous switching signal σ_m is defined as [6]

$$\sigma_m \triangleq \begin{cases} 1 & q \in \mathcal{Q}_m \\ 0 & q \notin \mathcal{Q}_m \end{cases}$$
 (3)

 $\forall m \in \mathcal{M}$, where $\mathcal{Q}_m \subset \mathcal{Q}$ denotes the regions in which muscle group m is able to supply a positive torque about the crank. The union of all muscle regions establishes the combined FES region of the crank cycle, defined as $Q_M \triangleq \bigcup_{m \in \mathcal{M}} Q_m$, and the kinematic deadzone (KDZ) region as the remainder $Q_K \triangleq Q \backslash Q_M$. By appropriately designing the switching signals in (3), each muscle is stimulated in kinematically efficient regions (i.e., at a high torque transfer ratio from muscle to crank) to delay fatigue. As different muscles are activated through their respective switching signals, the torque input to the system discretely changes; however, the states continuously evolve. The combination of discretely changing control inputs with continuous state dynamics gives rise to a state-dependent switched system. The switched system dynamics in (1) have the following properties [6].

Property 1. Parameter bounds: There exist known constants c_m , c_M , c_C , c_G , c_{P1} , c_{P2} , c_b , $c_d \in \mathbb{R}_{>0}$ such that $c_m \leq M \leq c_M$; $|C| \leq c_C |\dot{q}|$; $|G| \leq c_G$; $|P| \leq c_{P1} + c_{P2} |\dot{q}|$; $b \leq c_b$; $|d| \leq c_d$.

Property 2. Linear in the parameters: The functions M, C, G, and b are linearly parameterizable.

Property 3. Skew symmetry: The function \dot{M} and C satisfy $\dot{M} - 2C = 0, \ \forall q \in \mathcal{Q}$.

Property 4. Control effectiveness: When $q \in \mathcal{Q}_M$, the lumped switched unknown muscle control effectiveness is bounded by $B_{\underline{m}} \leq B_m \leq B_{\overline{m}}$, where $B_{\underline{m}}$, $B_{\overline{m}} \in \mathbb{R}_{>0}$ are known constants.

III. CONTROL DEVELOPMENT

In the following section, two controllers are developed, a robust sliding-mode cadence controller for the rider's muscles and an adaptive NN admittance controller for the cycle's motor.

A. Cadence Controller

Although the cadence controller has the same form as in [6], a new stability analysis is required (see Section IV) because a new objective is presented (i.e., admittance tracking). For clarity, the cadence tracking errors and the controller are presented here. The cycle's cadence is regulated using the rider's muscles in the FES regions and quantified by the tracking errors $e: \mathbb{R}_{\geq 0} \to \mathbb{R}$ and $r: \mathbb{R}_{\geq 0} \to \mathbb{R}$, each defined as²

$$e \triangleq q_d - q,$$
 (4)

$$r \triangleq \dot{e} + \alpha e,$$
 (5)

²For notational brevity, all functional dependencies are hereafter suppressed unless required for clarity of exposition.

where $q_d: \mathbb{R}_{\geq 0} \to \mathbb{R}$ denotes the desired position, designed to be sufficiently smooth (i.e., q_d , \dot{q}_d , $\ddot{q}_d \in \mathcal{L}_{\infty}$), and $\alpha \in \mathbb{R}_{>0}$ denotes a selectable constant control gain. The open-loop cadence error system is obtained by taking the derivative of (5), multiplying by M, adding and subtracting e, and substituting (1), (2), (4), and (5) to yield

$$M\dot{r} = \chi_1 - B_m u_h - \tau_e - Cr - e,\tag{6}$$

where the lumped auxiliary signal $\chi_1: \mathbb{R}^2 \times \mathbb{R}_{\geq 0} \to \mathbb{R}$ is defined as $\chi_1 \triangleq M\left(\ddot{q}_d + \alpha r - \alpha^2 e\right) + C\left(\dot{q}_d + \alpha e\right) + G + P + b\left(\dot{q}_d - r + \alpha e\right) + d + e$ and bounded by Property 1 as $|\chi_1| \leq c_1 + c_2 \, ||z|| + c_3 \, ||z||^2$, where $c_1, \ c_2 \ c_3 \in \mathbb{R}_{>0}$ are known constants, and the error vector $z \in \mathbb{R}^2$ is defined as $z \triangleq \begin{bmatrix} e \ r \end{bmatrix}^T$. Based on (6) and the subsequent stability analysis, the cadence controller is designed as

$$u_h = \frac{1}{B_{\underline{m}}} \Big(k_1 r + \Big(k_2 + k_3 \|z\| + k_4 \|z\|^2 \Big) \operatorname{sgn}(r) \Big),$$
(7)

where $k_i \in \mathbb{R}_{>0} \ \forall i=1,\ 2,\ 3,\ 4$ denote constant control gains, $\|\cdot\|$ denotes the standard Euclidean norm, $\mathrm{sgn}(\cdot)$ denotes the signum function, and $B_{\underline{m}}$ is introduced in Property 4. Substituting (7) into (6) yields the closed-loop cadence error system

$$M\dot{r} = \chi_{1} - \tau_{e} - Cr - e - \frac{B_{m}}{B_{\underline{m}}} \left(k_{1}r + \left(k_{2} + k_{3} \|z\| + k_{4} \|z\|^{2} \right) \operatorname{sgn}(r) \right).$$
(8)

B. Adaptive Admittance Controller

While the rider's muscles regulate cadence, an interaction torque error is introduced, quantified by $e_{\tau}: \mathbb{R}_{\geq 0} \to \mathbb{R}$, and defined as

$$e_{\tau} \stackrel{\triangle}{=} \tau - \tau_d,$$
 (9)

where $\tau_d: \mathbb{R}_{\geq 0} \to \mathbb{R}$ denotes the desired bounded interaction torque and $\tau: \mathbb{R}_{\geq 0} \to \mathbb{R}$ denotes the bounded measurable interaction torque between the cycle and rider (i.e., $\tau \in \mathcal{L}_{\infty}$) [16], [23]. By implementing an admittance filter, the interaction torque error can be transformed into an admittance error (i.e., a modified position and cadence error), which can be regulated using an inner-loop position controller. The admittance filter is given by

$$e_{\tau} \triangleq M_d \ddot{q}_a + B_d \dot{q}_a + K_d q_a, \tag{10}$$

where M_d , B_d , $K_d \in \mathbb{R}_{>0}$ denote constant filter parameters, selected such that the transfer function of (10) is passive (i.e., q_a , \dot{q}_a , $\ddot{q}_a \in \mathcal{L}_{\infty}$) [24, Lemma 6.4]; and q_a , \dot{q}_a , \ddot{q}_a : $\mathbb{R}_{\geq 0} \to \mathbb{R}$ denote the generated admitted position, velocity, and acceleration, respectively. To track the admitted trajectory, an adaptive inner-loop position controller is designed to regulate the admittance error system, quantified by $\xi: \mathbb{R}_{\geq 0} \to \mathbb{R}$ and $\psi: \mathbb{R}_{\geq 0} \to \mathbb{R}$, and defined as

$$\xi \triangleq q_a + q_d - q, \tag{11}$$

$$\psi \triangleq \dot{\xi} + \beta \xi, \tag{12}$$

where $\beta \in \mathbb{R}_{>0}$ denotes a constant control gain. The openloop admittance error system is generated by taking the time derivative of (12), multiplying by M, adding and subtracting ξ , and substituting (1), (11), and (12) to yield

$$M\dot{\psi} = Y\theta + d + P - C\psi$$

$$-B_{m}u_{h} - B_{e}u_{e}, \qquad (13)$$

$$Y\theta \triangleq M\left(\ddot{q}_{a} + \ddot{q}_{d} + \beta\psi - \beta^{2}\xi\right)$$

$$+C\left(\dot{q}_{a} + \dot{q}_{d} + \beta\xi\right) + G$$

$$+b\left(\dot{q}_{a} + \dot{q}_{d} - \psi + \beta\xi\right), \qquad (14)$$

where $Y: \mathbb{R}^2 \times \mathbb{R}_{\geq 0} \to \mathbb{R}^{1 \times 7}$ denotes a computable regression matrix (LP by Property 2), and $\theta \in \mathbb{R}^{7 \times 1}$ denotes a matrix of constant system parameters. To facilitate the subsequent analysis, (13) is further modified by adding and subtracting ξ and $f_m u_h$, yielding

$$M\dot{\psi} = Y\theta + \chi_2 - \xi - C\psi - B_e u_e + (S - f_m) u_h,$$
 (15)

where $f_m \triangleq B_m \left(\sin^2 \left(q_d + q_a \right), \ \dot{q}_d + \dot{q}_a \right)$. The $\sin^2 \left(\cdot \right)$ function is utilized to supply a bounded input to the NN, as well as shape the input to match the positive torque contribution of both legs. The auxiliary function χ_2 : $Q \times \mathbb{R} \times \mathbb{R}_{>0} \to \mathbb{R}$ is defined as $\chi_2 \triangleq P + \xi + d$, and bounded by Property 1 as $|\chi_2| \leq c_4 + c_5 \|\phi\|$, where $c_4, c_5 \in \mathbb{R}_{>0}$ are known constants, and the error vectors $\phi \in \mathbb{R}^3$, $\zeta \in \mathbb{R}^2$ are defined as $\phi \triangleq \begin{bmatrix} \zeta^T \ \dot{q}_a \end{bmatrix}^T$ and $\zeta \triangleq \begin{bmatrix} \xi \ \psi \end{bmatrix}^T$. The auxiliary function $S: \mathbb{R}^2 \to \mathbb{R}$ in (15) is defined as $S \triangleq f_m - B_m$ and can be bounded using the Mean Value Theorem [25] and Property 4 as $|S| \leq c_6 + c_7 \|\zeta\|$, where $c_6, c_7 \in \mathbb{R}_{>0}$ are known constants. Knowing $q_d,\ \dot{q}_d,\ q_a,\ \dot{q}_a\in \mathcal{L}_{\infty},$ let $\mathbb S$ be a compact simply connected set of $\mathbb R^3$ with map $f_m: \mathbb{S} \to \mathbb{R}$, where f_m is continuous. Then, there exist weights and thresholds such that the function $f_m(x_d)$ can be represented by a neural network as [26], [27]

$$f_m = W^T \rho \left(V^T x_d \right) + \epsilon \left(x_d \right), \tag{16}$$

where $x_d \triangleq \begin{bmatrix} 1 & \sin^2{(q_d + q_a)} & \dot{q}_d + \dot{q}_a \end{bmatrix}^T \in \mathbb{S}, \ V \in \mathbb{R}^{3 \times L}$ and $W \in \mathbb{R}^{(L+1) \times 1}$ are bounded constant ideal weight matrices of the neural network, and L is the number of neurons in the hidden layer. The function $\rho: \mathbb{R}^L \to \mathbb{R}^{L+1}$ is defined as $\rho \triangleq \begin{bmatrix} 1 & \rho_1 & \rho_2 & \dots & \rho_L \end{bmatrix}^T$, where $\rho_i, \ \forall i = \{1, \ 2, \ \dots, \ L\}$ represents the activation function for each neuron, and the function reconstruction error is denoted by $\epsilon: \mathbb{S} \to \mathbb{R}$.

Assumption 1. By [28] and Property 4, B_m is continuous and analytic on a compact set except at known locations of discontinuities (i.e., σ_m transitions at known locations based on a present muscle activation strategy). Accordingly, based on the design of the discrete switching signals in (3), B_m is right-continuous with finite jumps at known

locations. Following a development similar to [27, Theorem 3.1.5], sigmoidal jump approximation functions can be employed within the neural network to estimate the jumps. For simplicity, within the current development, the jumps are approximated by continuous functions and combined within the structure of the activation function ρ and the error is captured within ϵ in (16).

Since the weights W and V are unknown, an approximated version of (16) is generated as

$$\hat{f}_m \triangleq \hat{W}^T \rho \left(\hat{V}^T x_d \right), \tag{17}$$

where $\hat{V}: \mathbb{R}_{\geq 0} \to \mathbb{R}^{3 \times L}$ and $\hat{W} \in : \mathbb{R}_{\geq 0} \to \mathbb{R}^{(L+1) \times 1}$ are the estimates of V and W, respectively. To facilitate the following development, let the notation $\tilde{(\cdot)} \triangleq (\cdot) - \hat{(\cdot)}$ denote estimation errors, then $\rho\left(V^T x_d\right)$ may be approximated at $\rho\left(\hat{V}^T x_d\right)$ using a Taylor series expansion as

$$\rho\left(V^{T}x_{d}\right) = \hat{\rho} + \hat{\rho}'\tilde{V}^{T}x_{d} + \mathcal{O}^{2},\tag{18}$$

where
$$\hat{\rho} \triangleq \rho \left(\hat{V}^T x_d \right), \ \hat{\rho}' \triangleq \left. \frac{\partial \rho \left(V^T x_d \right)}{\partial V^T x_d} \right|_{\hat{V}^T x_d}$$
 denotes the

partial derivative, and O^2 denotes the higher order terms of the expansion.

Assumption 2. The ideal weights, thresholds, function approximation error of (16), and higher order terms of (18) are assumed to be bounded.

Based on (15) and the subsequent stability analysis, the admittance controller is designed as

$$u_{e} \triangleq \frac{1}{B_{e}} \left(Y \hat{\theta} + k_{5} \psi - \hat{f}_{m} u_{h} + \left(k_{6} + k_{7} \| \phi \| + (k_{8} + k_{9} \| \zeta \|) |u_{h}| \right) \operatorname{sgn}(\psi) \right), \tag{19}$$

where $k_i \ \forall i \in \{5, 6, ..., 9\} \in \mathbb{R}_{>0}$ denote constant control gains; $|u_h| \triangleq \frac{1}{B_m} \Big[k_1 \, |r| + k_2 + k_3 \, \|z\| + k_4 \, \|z\|^2 \Big]$; and $\hat{\theta} : \mathbb{R}_{\geq 0} \to \mathbb{R}^{7 \times 1}$ denotes an estimate of the constant system parameters. Substituting (19) into (15), adding and subtracting $\left(W^T \hat{\rho} + \hat{W}^T \hat{\rho}' \tilde{V}^T x_d \right) u_h$, utilizing (18), and performing some algebraic manipulation yields the closed-loop admittance error system

$$M\dot{\psi} = Y\tilde{\theta} - \xi - C\psi - k_5\psi - \left(k_6 + k_7 \|\phi\| + \left(k_8 + k_9 \|\zeta\|\right) |u_h|\right) \operatorname{sgn}(\psi) - \left(\tilde{W}^T \hat{\rho} + \hat{W}^T \hat{\rho}' \tilde{V}^T x_d - N\right) u_h + \chi_2, \tag{20}$$

where $\tilde{\theta}: \mathbb{R}_{\geq 0} \to \mathbb{R}^{7 \times 1}$ denotes the error between the actual and estimated system parameters, and the auxiliary function $N: \mathbb{R}^3 \to \mathbb{R}$ is defined as

$$N \triangleq S - \epsilon - \tilde{W}^T \hat{\rho}' \tilde{V}^T x_d - W^T \mathcal{O}^2. \tag{21}$$

Based on the subsequent stability analysis, the estimates for the system parameters in (14) and the neural network weights in (17) are generated on-line as

$$\dot{\hat{\theta}} = \operatorname{proj}\left(\Gamma_1 Y^T \psi\right),$$
 (22)

$$\dot{\hat{W}} = \operatorname{proj}\left(-\Gamma_2 \hat{\rho} u_h \psi\right), \tag{23}$$

$$\dot{\hat{V}} = \operatorname{proj}\left(-\Gamma_3 x_d u_h \psi \hat{W}^T \hat{\rho}'\right), \tag{24}$$

where $\Gamma_1 \in \mathbb{R}^{7 \times 7}$, $\Gamma_2 \in \mathbb{R}^{(L+1) \times (L+1)}$, $\Gamma_3 \in \mathbb{R}^{3 \times 3}$ denote constant positive definite learning gains, and $\operatorname{proj}(\cdot)$ denotes a projection algorithm [29, Section 4.4].

Property 5. By the Mean Value Theorem, Assumption 1, and the projection algorithm, $|N| \leq c_8 + c_7 \|\zeta\|$ for any combination of switching signals, where $c_8 \in \mathbb{R}_{>0}$ is a known constant and c_7 was introduced above.

IV. STABILITY ANALYSIS

To facilitate the following theorems, let $V_1: \mathbb{R}^2 \to \mathbb{R}$ denote a continuously differentiable, positive definite storage function defined as

$$V_1 \triangleq \frac{1}{2}Mr^2 + \frac{1}{2}e^2,$$
 (25)

and let $V_2:\mathbb{R}^{4L+10}\to\mathbb{R}$ denote a continuously differentiable, positive definite Lyapunov function candidate defined as

$$\begin{split} V_2 &\triangleq \frac{1}{2}M\psi^2 + \frac{1}{2}\xi^2 + \frac{1}{2}\tilde{\theta}^T\Gamma_1^{-1}\tilde{\theta} \\ &\quad + \frac{1}{2}\left(\tilde{W}^T\Gamma_2^{-1}\tilde{W} + \operatorname{tr}\left(\tilde{V}^T\Gamma_3^{-1}\tilde{V}\right)\right), \quad (26) \end{split}$$

where $tr(\cdot)$ is the trace of a matrix.

Theorem 1. Given the closed-loop cadence error system in (8), when $q \in \mathcal{Q}_M$, the cadence controller is passive from input $|\tau_e|$ to output |r|, $\forall t$ provided the following constant gain conditions are satisfied: $k_2 \geq c_1$, $k_3 \geq c_2$, $k_4 \geq c_3$.

Proof: Because of the discontinuity in the muscle controller in (7), the time derivative of V_1 exists almost everywhere (a.e.) (i.e., for almost all $t \in [t_0, \infty)$). After substituting (5), (8), using Properties 1, 3, and 4, and upper bounding, the time derivative of (25) can be expressed as

$$\dot{V}_1 \stackrel{\text{a.e.}}{\leq} -\alpha e^2 - k_1 r^2 + |r| |\tau_e|,$$
 (27)

provided the aforementioned gain conditions are satisfied. Because the interaction torque is bounded, from the perspective of the rider, the physically applied motor torque is similarly bounded. Hence, by [24, Definition 6.3] the cadence error system is output strictly passive with input $|\tau_e|$, output |r|, storage function V_1 , and the cadence controller is bounded (i.e., $u_h \in \mathcal{L}_{\infty}$).

Theorem 2. Given the closed-loop error system in (20) and the admittance relation in (10), the admittance error system is globally asymptotically stable in the sense that $\|\zeta\| \to 0$

as $t \to \infty$, provided the following constant gain conditions are satisfied: $k_6 \ge c_4$, $k_7 \ge c_5$, $k_8 \ge c_7$, $k_9 \ge c_8$.

Proof: Similar to Theorem 1, because of the discontinuity in the admittance controller in (19), the time derivative of (26) exists almost everywhere. After substituting (12) and (20), using Properties 1, 3, and 4, inserting the update laws in (22)-(24), and upper bounding, the time derivative of (26) can be expressed as

$$\dot{V}_2 \stackrel{\text{a.e.}}{\le} -\beta \xi^2 - k_5 \psi^2,$$
 (28)

provided the aforementioned gain conditions are satisfied. Hence, (26) has a negative semi-definite derivative across both the FES and KDZ regions. Subsequently, [30] can be invoked, along with the radially unboundedness of (26), to show $|\xi|, |\psi|, ||\zeta|| \to 0$ as $t \to \infty$. Since $V_2 > 0$ and $\dot{V}_2 \leq 0$, $V_2 \in \mathcal{L}_{\infty}$. Hence, $\xi, \psi, \tilde{\theta} \in \mathcal{L}_{\infty}$, which implies $\dot{q}, \hat{\theta} \in \mathcal{L}_{\infty}$. Since (10) is passive, $\dot{q}_a, \ddot{q}_a \in \mathcal{L}_{\infty}$, which implies $Y, ||\phi||, x_d \in \mathcal{L}_{\infty}$. By (23), (24), and $x_d \in \mathcal{L}_{\infty}$, $\hat{f}_m \in \mathcal{L}_{\infty}$. Finally, because $u_h \in \mathcal{L}_{\infty}$ by Theorem 1, $u_e \in \mathcal{L}_{\infty}$.

V. EXPERIMENTS

A. Experimental Testbed

Please refer to [13] for details of the instrumented motorized FES cycle.

B. Experimental Methods

Two experimental protocols were conducted on one ablebodied male participant aged 26, in random order. Protocol A ran the controllers in (7) and (19), and Protocol B disabled both the NN feedforward and adaptive feedforward components of (19). The purpose of such a design was to isolate the contribution of the feedforward components of the cycle's motor controller. Each protocol had a total duration of 180 seconds, with the first 30 seconds consisting of a smooth motor-only ramp to the desired cadence of 50 RPM using (19), i.e., with the admittance controller active. After the initial ramp, the controller in (7) was switched on, the rider was stimulated, and steady-state (SS) errors were recorded. For all experiments, the participant was blind to the desired trajectories for the duration of the experiment. The experimental protocols were approved by the Institutional Review Board at the University of Florida. For all experiments, the admittance parameters in (9) and (10) were selected as $K_d =$ $0 \frac{\text{Nm}}{\text{rad}}, \ B_d = 2 \frac{\text{Nm·s}}{\text{rad}}, \ M_d = 2 \frac{\text{Nm·s}^2}{\text{rad}}, \ \text{and} \ \tau_d \in [0, \ 0.2] \ \text{Nm}.$ The activation function of the NN was selected as the softplus function, $\rho(x) \triangleq \ln(1 + \exp(x))$, and the number of neurons was set to 5 (i.e., L = 5).

C. Results and Discussion

Table I provides details on the average and standard deviation of the measured cadence, admitted cadence, admittance cadence error, and estimated power production by the rider, calculated at steady state (i.e., after the initial cadence ramp to 50 RPM). The average estimated power

Table I Experimental results, reported as average \pm standard deviation

Protocol	<i>q</i> (RPM)*	$\dot{q}_{lpha} \; ({ m RPM})^{\dagger}$	$\dot{\xi}$ (RPM)	\hat{P} (W)
A	48.84±1.87	-1.24±1.49	-0.08±1.30	3.31±2.79
В	49.04±1.90	-1.15±1.30	-0.19±1.53	3.22±2.72

*At SS, the average cadence error is given as $\dot{e}=50-\dot{q}$. $\dagger \dot{q}_{\alpha}:\mathbb{R}_{\geq0}\to\mathbb{R}$ denotes the average admitted cadence defined as $\dot{q}_{\alpha}\triangleq\dot{q}_{d}+\dot{q}_{a}$.

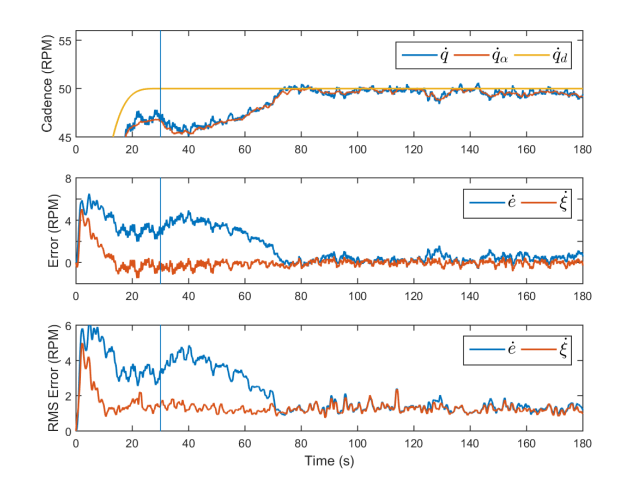


Figure 1. Protocol A: (Top) The actual, admitted, and desired cadence; (Middle) cadence errors; and (Bottom) RMS cadence errors, with the vertical lines representing the time of activation of (7).

production is denoted by $\hat{P}: \mathbb{R}_{\geq 0} \to \mathbb{R}$, which is defined as $\hat{P} \triangleq \text{mean}\left(\dot{q}\right) \left(\text{mean}\left(\tau\right) - \tau_{p}\right)$, where $\tau_{p}: \mathbb{R}_{\geq 0} \to \mathbb{R}$ denotes an estimate of the passive torque required to actuate the combined rider-cycle system at the desired cadence, collected during each trial for 4.8 seconds prior to controller activation (i.e., approximately four crank cycles at 50 RPM). Figure 1 displays cadence tracking results, including errors and root-mean-squared (RMS) errors, and for visual clarity, a one second moving average filter was applied.

Prior to the muscle controller in (7) being activated, the rider's legs act as a drag on the system, generating negative torque, and therefore decreasing the admitted cadence. Because only the admitted error system is being regulated at this point, the position error e begins to accumulate; therefore, when the muscle controller in (7) is activated, a nonzero stimulation is applied. Under normal circumstances, this error accumulation would be undesirable, however, because the rider's muscles do not generate torque at low levels of stimulation, this effect becomes desirable to "prime" the muscles for torque generation. By applying low stimulation levels and increasing them over the course of the experiment, torque production is gradually increased and results in a more comfortable experience for the rider. Furthermore, by decreasing the derivative gain k_1 on muscle stimulation, sharp increases in stimulation are avoided due to system disturbances, and again, the rider experiences a smoother

stimulation pattern. As the stimulation level increases, the rider's leg muscles are gradually able to produce the desired amount of torque (at $t\approx 70~\mathrm{s}$) and due to the admittance filter in (10), the admitted trajectory begins to align with the desired, resulting in a less error accumulation (i.e., e) and a less aggressive ramp in the stimulation input. As the muscles begin to fatigue, their cumulative torque production lessens and the admitted trajectory begins to decrease; consequently, the stimulation input increases to maintain torque levels. At t=30~s, the update laws for both $\hat{\theta}$ and \hat{f}_m are activated and the estimate begin to evolve. The adaptive and NN feedforward components simultaneously estimate system dynamics, and affect each other over time; therefore, the gains on the adaptive gradient component were set significantly higher than those of the NN to learn on two different time scales.

To demonstrate the effect of the feedforward components of (19), the adaptive gradient and NN components were disabled (i.e., Protocol B). As illustrated by Table I, using adaptation results in the admittance cadence error $\dot{\xi}$ being reduced by 58%, with the standard deviation of the admittance cadence error being reduced by 15%. Despite the reduction in error, the average control inputs to the motor were similar, with similar torque production by the rider.

VI. CONCLUSION

An adaptive NN admittance controller was successfully developed for an FES cycle to promote rehabilitation in individuals with NCs. The adaptive component of the admittance controller estimated the parameters within the dynamics while the NN component estimated the muscle control effectiveness. Stability of the combined cycle-rider system was proven with a Lyapunov-like switched systems stability analysis and the efficacy of the proposed controller was demonstrated through experiments with and without adaptation on one able-bodied participant. Future works will involve conducting additional experiments on people with NCs and accounting for stimulation saturation.

REFERENCES

- [1] S. E. Wallace and M. L. Kimbarow, *Cognitive Communication Disorders*. Plural Publishing, 2016.
- [2] E. J. Benjamin, M. J. Blaha, S. E. Chiuve, M. Cushman, S. R. Das, R. Deo, S. D. de Ferranti, J. Floyd, M. Fornage *et al.*, "Heart disease and stroke statistics - 2017 update," *Circulation*, vol. 135, no. 10, pp. 146–603, 2017.
- [3] "Spinal cord injury facts and figures at a glance," J. Spinal Cord Med., 2017.
- [4] T. Mohr, J. Pødenphant, F. Biering-Sørensen, H. Galbo, G. Thamsborg, and M. Kjær, "Increased bone mineral density after prolonged electrically induced cycle training of paralyzed limbs in spinal cord injured man," *Calcif. Tissue Int.*, vol. 61, no. 1, pp. 22–25, 1997.
- [5] S. Ferrante, A. Pedrocchi, G. Ferrigno, and F. Molteni, "Cycling induced by functional electrical stimulation improves the muscular strength and the motor control of individuals with post-acute stroke," *Eur. J. Phys. Rehabil. Med.*, vol. 44, no. 2, pp. 159–167, 2008.
- [6] M. J. Bellman, R. J. Downey, A. Parikh, and W. E. Dixon, "Automatic control of cycling induced by functional electrical stimulation with electric motor assistance," *IEEE Trans. Autom. Science Eng.*, vol. 14, no. 2, pp. 1225–1234, April 2017.
- [7] K. J. Hunt, J. Fang, J. Saengsuwan, M. Grob, and M. Laubacher, "On the efficiency of FES cycling: A framework and systematic review," *Technol. Health Care*, vol. 20, no. 5, pp. 395–422, 2012.

- [8] S. Jezernik, R. G. Wassink, and T. Keller, "Sliding mode closed-loop control of FES controlling the shank movement," *IEEE Trans. Biomed. Eng.*, vol. 51, no. 2, pp. 263–272, 2004.
- [9] C. Cousin, V. H. Duenas, C. Rouse, and W. E. Dixon, "Motorized functional electrical stimulation for torque and cadence tracking: A switched Lyapunov approach," in *Proc. IEEE Conf. Decis. Control*, 2017, pp. 5900–5905.
- [10] M. J. Bellman, T. H. Cheng, R. J. Downey, C. J. Hass, and W. E. Dixon, "Switched control of cadence during stationary cycling induced by functional electrical stimulation," *IEEE Trans. Neural Syst. Rehabil. Eng.*, vol. 24, no. 12, pp. 1373–1383, 2016.
- [11] V. H. Duenas, C. Cousin, V. Ghanbari, and W. E. Dixon, "Passivity-based learning control for torque and cadence tracking in functional electrical stimulation (FES) induced cycling," in *Proc. Am. Control Conf.*, 2018, pp. 3726–3731.
- [12] V. Duenas, C. Cousin, A. Parikh, and W. E. Dixon, "Functional electrical stimulation induced cycling using repetitive learning control," in *Proc. IEEE Conf. Decis. Control*, 2016.
- [13] V. H. Duenas, C. A. Cousin, A. Parikh, P. Freeborn, E. J. Fox, and W. E. Dixon, "Motorized and functional electrical stimulation induced cycling via switched repetitive learning control," *IEEE Trans. Control Syst. Tech.*, to appear, DOI: 10.1109/TCST.2018.2827334.
- [14] H. Lee and N. Hogan, "Essential considerations for design and control of human-interactive robots," in *IEEE Int. Conf. Robot. Autom.*, 2016, pp. 3069–3074.
- [15] I. Ranatunga, F. L. Lewis, D. O. Popa, and S. M. Tousif, "Adaptive admittance control for human-robot interaction using model reference design and adaptive inverse filtering," *IEEE Trans. Control Sys. Tech.*, vol. 25, no. 1, pp. 278–285, 2017.
- [16] Y. Li and S. S. Ge, "Impedance learning for robots interacting with unknown environments," *IEEE Trans. Control Sys. Tech.*, vol. 22, no. 4, pp. 1422–1432, 2014.
- [17] H. I. Krebs, B. T. Volpe, D. Williams, J. Celestino, S. K. Charles, D. Lynch, and N. Hogan, "Robot-aided neurorehabilitation: a robot for wrist rehabilitation," *IEEE Trans. Neur. Syst. Rehab. Eng.*, vol. 15, no. 3, pp. 327–335, 2007.
- [18] A. J. Del-Ama, A. D. Koutsou, J. C. Moreno, A. De-Los-Reyes, Á. Gil-Agudo, and J. L. Pons, "Review of hybrid exoskeletons to restore gait following spinal cord injury," *J. Rehabil. Res. Dev.*, vol. 49, no. 4, pp. 497–514, 2012.
- [19] F. Anaya, P. Thangavel, and H. Yu, "Hybrid FES-robotic gait rehabilitation technologies: a review on mechanical design, actuation, and control strategies," *Int. J. Intell. Robot. Appl.*, pp. 1–28, 2018.
- [20] C. Cousin, V. H. Duenas, C. Rouse, and W. E. Dixon, "Stable cadence tracking of admitting functional electrical stimulation cycle," in *Proc.* ASME Dyn. Syst. Control Conf., 2018.
- [21] C. A. Cousin, V. Duenas, C. Rouse, and W. E. Dixon, "Admittance control of motorized functional electrical stimulation cycle," in *Proc.* IFAC Conf. Cyber. Phys. Hum. Syst., 2018, pp. 328–333.
- [22] C. Cousin, V. H. Duenas, C. Rouse, and W. E. Dixon, "Cadence and admittance control of a motorized functional electrical stimulation cycle," in *Proc. IEEE Conf. Decis. Control*, Dec. 2018, pp. 6470–6475.
- [23] K. P. Tee, R. Yan, and H. Li, "Adaptive admittance control of a robot manipulator under task space constraint," in *IEEE Int. Conf. Robot. Autom.* IEEE, 2010, pp. 5181–5186.
- [24] H. K. Khalil, Nonlinear Systems, 3rd ed. Upper Saddle River, NJ: Prentice Hall, 2002.
- [25] A. Behal, W. E. Dixon, B. Xian, and D. M. Dawson, Lyapunov-Based Control of Robotic Systems. CRC Press, 2009.
- [26] F. L. Lewis, "Nonlinear network structures for feedback control," Asian J. Control, vol. 1, no. 4, pp. 205–228, 1999.
- [27] F. L. Lewis, R. Selmic, and J. Campos, Neuro-Fuzzy Control of Industrial Systems with Actuator Nonlinearities. Philadelphia, PA, USA: Society for Industrial and Applied Mathematics, 2002.
- [28] N. Sharma, K. Stegath, C. M. Gregory, and W. E. Dixon, "Nonlinear neuromuscular electrical stimulation tracking control of a human limb," *IEEE Trans. Neural Syst. Rehabil. Eng.*, vol. 17, no. 6, pp. 576–584, Jun. 2009.
- [29] W. E. Dixon, A. Behal, D. M. Dawson, and S. Nagarkatti, Nonlinear Control of Engineering Systems: A Lyapunov-Based Approach. Birkhauser: Boston, 2003.
- [30] R. Kamalapurkar, J. A. Rosenfeld, A. Parikh, A. R. Teel, and W. E. Dixon, "Invariance-like results for nonautonomous switched systems," *IEEE Trans. Autom. Control*, vol. 64, no. 2, pp. 614–627, Feb. 2019.